ISTITUTO NAZIONALE DI GEOFISICA E VULCANOLOGIA

ACCEPTED ON ANNALS OF GEOPHYSICS, 61, 2018; Doi: 10.4401/ag-7839

Equilibrium Viscosity and Disequilibrium Rheology of a high Magnesium Basalt from Piton De La Fournaise volcano, La Reunion, Indian Ocean, France

Stephan Kolzenburg, Daniele Giordano, Andrea Di Muro, D. B. Dingwell

Equilibrium Viscosity and Disequilibrium Rheology of a high Magnesium Basalt from Piton De La Fournaise volcano, La Reunion, Indian Ocean, France

S. Kolzenburg[1,2,3]*, D. Giordano[3,4,5], A. Di Muro[6], D.B. Dingwell[1]

1) Ludwig-Maximilians-University Munich, Department of Earth and Environmental Sciences, Theresienstr. 41, 80333 Muenchen, Germany

2) McGill University, Department of Earth and Planetary Sciences, 3450 University Street, H3A 0E8 Montreal, Quebec, Canada

3) Universita degli Studi di Torino, Dipartimento di Scienze della Terra, Via Valperga Caluso 35, 10125 Torino, Italy

4) Istituto Nazionale di Geofisica e Vulcanologia-Sezione di Pisa, Via della Faggiola, 32, 56126 Pisa, Italy.

5) Institute of Geoscience and Earth Resources (IGG-CNR), Italian National Research Council (CNR), Pisa, Italy

6) Institut de Physique du Globe de Paris, Observatoire Volcanologique du Piton de la Fournaise, 1 Rue Jussieu, 75005 Paris, France

Submitted to: Annals of Geophysics

Special volume: "MeMoVolc"

* Corresponding author: Stephan Kolzenburg; skolzenburg@gmail.com

Keywords: Rheology; Crystallization Kinetics; Lava Flow; Piton de la Fournaise; La Reunion; disequilibrium processes; high Mg-basalt.

Abstract

Lava flows are a common hazard at basaltic to intermediate volcanoes and have posed a significant threat to La Reunion Island over the past centuries. In sustained flow units, the efficiency of lava transport away from the vent is dominated by cooling. For basaltic to intermediate lavas, it is the ability of the lava to solidify during cooling which exerts a first-order control on spatial extent and flow distance. As a consequence, understanding the *sub-liquidus* rheology of lavas has become a key focus in lava flow research in the past decade. To date, the development of a systematic understanding of lava rheology during emplacement conditions has been significantly hampered by a lack of experimental data. Here we present new data on the rheological evolution of crystallizing high-Mg basalt from Piton de la Fournaise. Sub-liquidus experiments were performed at constant cooling rates ranging from 0.5 to 5 K/min. Those rates mimic thermal conditions experienced 1) by lava during flow on the surface and 2) by magma during dike and sill emplacement. Our data show that the effective viscosity of the crystallizing suspension increases until reaching a specific sub-liquidus temperature, the so-called "rheological cut-off temperature" (T_{cutoff}), at which the lava becomes rheologically immobile and flow ceases. This departure from the pure liquid viscosity curve to higher viscosity is a consequence of rapid crystallization and its variability for a given lava is found to be primarily controlled by the imposed cooling rate. Based on these experimental data, we adapt the failure forecasting method (FFM) - commonly used to describe the self-accelerating nature of seismic signals to forecast material failure - to predict the rheological cut-off temperature (T_{cutoff}). The presented data substantially expand the modest experimental database on non-equilibrium rheology of lavas and represent a step towards understanding the underlying process dynamics.

52 # 1. Introduction

1.1. Motivation and scope of this study

54 The flow of lava is dominantly governed by viscosity, effusion-rate and the slope and morphological features of the underlying topography (Cashman et al., 2013; Dragoni
56 et al., 1986; Hallworth et al., 1987; Harris and Rowland, 2001; Pinkerton, 1987). Mitigating the hazards posed by lava flows that threaten infrastructure has only shown
58 moderate success to date (Barberi et al., 2003). This is largely due to an incomplete understanding of how lava flows, how and when flows stop and is further hampered by a
60 lack of methods to provide up-to-date topographic surface models (Cashman et al., 2013; Farquharson et al., 2015; Favalli et al., 2010; James and Robson, 2014; Kolzenburg et al.,
62 2016a; Kolzenburg et al., 2018c). These shortfalls drastically reduce our ability to predict lava flow emplacement.

64 One of the most challenging aspects of predicting the flow dynamics of lavas is that the rheological properties of lava flows evolve during eruption and emplacement since they
66 occur under conditions that impose a state of dynamic disequilibrium. The transient nature of the rheological properties is caused by changes in the temperature, composition and
68 phase state of the lava or magma resulting from gas loss, cooling, crystallization and vesiculation. The importance of *non-isothermal* effects on the crystallization kinetics and
70 textural development of silicate melts have in principle been recognized for decades (Arzilli and Carroll, 2013; Coish and Taylor, 1979; Gamble and Taylor, 1980; Hammer,
72 2006; Lofgren, 1980; Long and Wood, 1986; Vetere et al., 2013; Walker et al., 1976). Yet experimental parameterisation of these effects on magma flow behaviour has lagged
74 behind badly. Such a detailed understanding of the rheological evolution of crystallizing

magmas or lavas requires direct measurement of the flow properties at emplacement conditions.

To date, direct measurements of the rheology of lavas or magmas under natural conditions are few (Belousov and Belousova, 2018; Chevrel et al., 2018; Einarsson, 1949; Gauthier, 1973; Panov et al., 1988; Pinkerton, 1994; Pinkerton and Norton, 1995; Pinkerton and Sparks, 1978; Shaw et al., 1968). They represent crucial measurements for benchmarking of experimental data. In conjunction with systematic laboratory studies on the evolution of lava flow properties as a function of the physico-chemical environmental conditions such data enable the production of new input parameters for predictive models of lava rheology and emplacement. In an effort to generate a systematic empirical database that will help to elucidate the systematics of the underlying processes, a range of concentric cylinder viscometry data has been presented in the past decade. Concentric cylinder viscometry typically utilises measurements of the torque exerted by the liquid on a spindle inserted into a sample melt and rotated at a constant rate. The available datasets can broadly be separated into measurements at constant, isothermal conditions (i.e. constant undercooling and at fixed shear rates and oxygen fugacities) e.g. (Chevrel et al., 2015; Ishibashi and Sato, 2007; Robert et al., 2014; Sato, 2005; Sehlke et al., 2014; Soldati et al., 2016; Vona et al., 2011; Vona et al., 2013) and measurements at constant cooling rates that map suspension rheology at varying experimental shear-rates and/or changing oxygen fugacity (Giordano et al., 2007; Kolzenburg et al., 2018a; Kolzenburg et al., 2018b; Kolzenburg et al., 2016b; Kolzenburg et al., 2017; Kouchi et al., 1986; Shaw et al., 1968). The former dataset aims at attaining mechanical and textural equilibrium and permit the sampling of the equilibrated material. These data are used to correlate the viscosity measurements to the sample textures. The latter dataset aims at reproducing natural flow

conditions and allows the quantification of the "rheological cut-off temperature" (T_{cutoff}), at which the lava becomes rheologically immobile and flow ceases. However, sampling of the texture or modelling of the change in crystal content throughout the experiment for correlation to the rheological data is not possible during these dynamic, disequilibrium experiments, since crystallization under these conditions occurs far from equilibrium and very rapidly.

Here we present new experimental data on a high-Mg Basalt from Piton de la Fournaise that investigate the sub liquidus evolution of melt rheology as a function of cooling rate at atmospheric conditions. While these data can also facilitate the understanding of kinetic flow evolution at thermal conditions (i.e. absolute temperature and cooling rates) of partly degassed magma during transport toward the surface in dike-swarms, the decrease in oxygen fugacity occurring at sub-surface conditions will likely require a shift of the presented data to lower temperatures, as shown in Kolzenburg et al. (2018a). Nevertheless, the presented dataset serves to expand a growing database on non-isothermal rheology, which is necessary for the development of empirical models of the effective lava viscosity at emplacement conditions. Such data are essential for robust prediction of lava flow behaviour and flow geometry.

1.2. Compositional characteristics of the 2007 eruption of Piton de la Fournaise.

Piton de la Fournaise volcano is located on La Reunion Island ~800 km east of Madagascar. In 2007, it produced one of its largest volume eruptions of the past centuries. A detailed account of the eruption can be found in Staudacher et al. (2009). The 2007 eruption represents an interesting end-member with respect to lava rheology since it erupted a wide range of basalt compositions and crystal contents, spanning almost the

entire range of magma compositions typically erupted at Piton de la Fournaise (Villemant et al., 2009). Based on regular sampling of the lava and compositional analyses, Staudacher et al. (2009) and Di Muro et al. (2014) report that the lava was, initially, evolved (MgO ca. 7wt%) and poorly phyric with less than 5 vol% of small olivine/clinopyroxene phenocrysts and plagioclase microlites. Throughout the eruption, the volume fraction (and size) and of olivine crystals increased, reaching up to 40 vol% of olivine phenocrysts at the end of the eruption (Di Muro et al., 2014; Staudacher et al., 2009; Villemant et al., 2009). Villemant et al. (2009) report that the April 2007 eruption produced some of the most primitive and most Mg-rich melts erupted at Piton de la Fournaise (MgO~9wt%) and that they correspond to the first step of the differentiation trend for the parental magma at Piton de la Fournaise (Albarède et al., 1997; Boivin and Bachèlery, 2009; Villemant et al., 2009). Villemant et al. (2009) and Di Muro et al. (2014) further note that early erupted lavas and the matrix glass of the 2007 lava flows (bulk MgO content ~25–30%) are less Mg-rich (MgO~6-%) than matrix glass of scoria (glass MgO content ~7% and bulk rock MgO content ~18–20%) or Pélé's hair (glass MgO content=7.5–9%) emitted at the same vent; see (Tables 1a–b) in Villemant et al. (2009). Melt inclusions trapped in the most Mg-rich olivines (Fo86) record mafic melt compositions (MgO 10-11 wt%) representative of the primary melts feeding the central and shallow plumbing system of Piton de la Fournaise (Di Muro et al., 2014). Average lava composition at Piton de la Fournaise record extensive early olivine+/-pyroxene fractionation at depth, while primitive magnesian melts (MgO > 14wt%) are never erupted on the La Réunion island (e.g. See Fretzdorff and Haase (2002), Di Muro et al. (2016) and references therein). In summary, the available data demonstrate that the magma is significantly more Mg-rich during subsurface transport and eruption than is preserved in

146 the lava flow matrix glass and thus that the formation of olivine ± clinopyroxene ± plagioclase plays a central role in the solidification of magma and lavas and, thereby their
148 rheological evolution at Piton de la Fournaise volcano.

2. Experimental Materials and Methodology

150 ### *2.1. Experimental Material and Melt Preparation*

The samples we selected from the 2007 eruption display relatively high crystal
152 contents (~25-40 vol%). For rheological experimentation we created a partial melt of the crystallized matrix and some amount of the crystal cargo. The rock sample was crushed
154 using a jaw crusher and fragments of ~ 1cm diameter were hand-picked for matrix melt separation. These fragments were then partially melted in large thin-walled Pt crucibles to
156 separate the olivine phenocrysts from the matrix. Melting was performed in a Nabertherm® $MoSi_2$ box furnace at 1250°C in multiple, small, batches for ~20 minutes per
158 batch. During re-melting, the dense olivine phenocrysts sank to the base and the interstitial melt percolated through the crystal framework, forming a lens of melt on top of the crystal
160 cumulate. This melt lens was carefully decanted to collect the interstitial partial melt. Fifteen batches were required to recover sufficient melt volume to perform viscometry.
162 The quenched melt batches were crushed and ground using an agate mortar and thoroughly mixed for homogenization. These powders were then re melted at 1350°C for 12h to
164 ensure chemical homogeneity. After homogenization the sample was quenched by pouring it onto a steel plate in order to ensure a cooling rate fast enough to supress crystal growth.
166 Visual assessment and Raman spectroscopy following the approach of Di Genova et al. (2018) affirmed that the glasses remained crystal-free. The glass was crushed and re-
168 melted into $Pt_{80}Rh_{20}$ cylindrical crucibles of 51 mm height and 26.6 mm diameter. The crucible was then transferred into a Deltech bottom-loading furnace adapted for

rheological experimentation, the device is described in successive configurations in (Dingwell, 1991; Dingwell, 1986; Dingwell, 1990; Dingwell, 1992).

2.2. Glass chemistry analysis

The bulk chemical composition of the experimental material was determined for the quenched glass using an electron probe micro analyser (EPMA). The sample was impregnated in a low viscosity epoxy resin, polished and carbon coated. The major element composition was determined at the Department of Earth and Environmental Sciences at the University of Munich, using a Cameca SX100 EPMA with 15 kV acceleration voltage and 5 nA beam current. In order to reduce the alkali volatilization the beam diameter was defocused down to 10 μm. Synthetic wollastonite (Ca, Si), periclase (Mg), hematite (Fe), corundum (Al), natural orthoclase (K), and albite (Na) were used as standards, and matrix correction was performed by PAP procedure (Pouchou and Pichoir, 1991). The accuracy was better than 2.5% for all analysed elements. Normalized results of the average of 10 EPMA analyses are presented in Table 1; analytical totals average 99.76 %.

2.3. Concentric Cylinder (CC) viscometry and Differential scanning calorimetry (DSC).

Glass transition temperatures at onset (Tg_{onset}) and peak (Tg_{peak}) were obtained from heat capacity curves derived from differential scanning calorimetry on aliquots of the re-melted glass undergoing cooling/heating cycles at rates of 5, 10, 15 and 20 °K/min. Reproducibility of both Tg_{onset} and Tg_{peak} are better than 0.5 % (i.e. ~3 °K); see also Giordano et al. (2015) and Giordano and Russell (2017). These data are used to recover the low temperature viscosity data using the method presented by Giordano et al. (2008a), that correlates Tg_{onset} and Tg_{peak} to fixed values of viscosity; these data are reported in Table 2.

194 High temperature rheological experiments were performed using a Brookfield DV-III+ viscometer head (full range of torque = 0 - 0.7187 mNm). A $Pt_{80}Rh_{20}$ spindle is 196 suspended from the viscometer head, immersed into the sample and rotated at a constant rate. The torque exerted by the sample at constant rotation rate is proportional to the melt 198 or suspension viscosity. The spindle head used in these experiments is 33.2 mm long with 14.4 mm diameter and a 45° conical top and bottom to reduce edge effects, this bob is hung 200 on a 2.4 mm diameter stem; see also: (Dingwell, 1986; Dingwell and Virgo, 1988). The torque reading for this spindle and crucible were calibrated against DGG1 standard glass, 202 with a known viscosity-temperature relationship (Meerlender, 1975). Calibration was performed for shear rates and temperatures exceeding those used in this study. The 204 precision of the viscosity determination is ±3% as described in Dingwell (1986). The thermal evolution of the sample at the imposed cooling rates was calibrated with an 206 accuracy of ±1 ℃ over the entire experimental temperature range using a platinum sheathed Type-S thermocouple immersed in DGG1 standard glass. The super liquidus melt viscosity 208 was measured at between 1444 and 1321 ℃ in temperature steps of ~25 K; see Table 2 (corresponding to furnace set points of 1450 - 1325 ℃). Each temperature step was 210 maintained for 120 min and a stable torque reading was commonly achieved after ~70 min, indicating thermal and chemical (i.e. redox) homogeneity.

212 The high temperature viscosity measurements in combination with the low temperature melt viscosity data recovered via application of a shift factor to the DSC data, 214 are used to fit a VFT-model (Tammann and Hesse, 1926) to the experimental data. This model describes the theoretical crystal-free liquid viscosity at sub-liquidus temperatures 216 (Giordano et al., 2008a; Gottsmann et al., 2002; Hess and Dingwell, 1996; Hess et al., 1995) and is used to calculate the relative viscosity of the suspension (see section 2.4 for

details). The model parameters are reported together with the liquid viscometry results in Table 2.

2.4. Non-Isothermal Concentric Cylinder (CC) viscometry.

Non-isothermal experimentation was performed following methods similar to the ones described in previous work (Giordano et al., 2007; Kolzenburg et al., 2018a; Kolzenburg et al., 2017). A series of experiments were run at constant cooling rates of 0.5, 1, 3 and 5 °K/min and an initial shear rate of 0.766 sec^{-1} (corresponding to 2.5 rpm). Experiments at lower initial shear rates were not possible for the given experimental temperatures because at low rotation rates, the surface tension of the melt in the meniscus between spindle and crucible is sufficiently high to pull the spindle to the sidewalls of the crucible. During experimentation, the measured torque increased as a function of the apparent viscosity of the suspension. Upon reaching the maximum torque limit of 0.7187 mNm, the shear rate was automatically dropped to 0.368, 0.184, 0.092, 0.061, 0.031 s-1 (1.2, 0.6, 0.3, 0.2, 0.1 rpm, respectively), each successive time the limit was reached.

Between consecutive dynamic cooling experiments the sample was re-heated to 1396 °C (corresponding to a furnace set point of 1400 °C) for a minimum of two hours and homogenized by stirring at a shear rate of 3.06 s^{-1} (10 rpm) in order to ensure complete melting of all crystalline phases formed during previous experimentation. After the end of the last experimental cycle, the sample was re-melted and quenched to a glass. Based on the results of Mysen and Virgo (1978) and Dingwell and Virgo (1987) we assume that redox equilibrium was achieved during the super-liquidus melt viscosity determination, which lasted more than 24 hours at atmospheric conditions. Since the crystallization experiments lasted between 0.5 and less than 5.8 hrs (at lower temperatures; i.e. higher

viscosities and slower redox equilibration) and we assume that the melt redox state was re-
242 equilibrated to the initial, pre-experimental state within the time spent at high temperature under constant stirring during remelting. The assumption of thermal and redox
244 equilibration and re-melting of previous crystal phases was confirmed by the recovery of a steady torque measurement at ±1% of the value of the pure melt over more than an hour.

246 In order to resolve the crystallization induced rheological deviation from the pure melt viscosity at greater detail than in absolute viscosity space we calculate the relative
248 viscosity η_r, that is the ratio between the measured shear viscosity of the mixture η_s of the crystallizing suspension and the liquid viscosity η_l, (Eq. 3):.

250 $$\eta_r = \frac{\eta_s}{\eta_l} \text{ (eq. 3)}$$

where η_l was calculated by employing a VFT-fitting of the low temperature
252 viscosity data reported in Table 2 and the super liquidus viscometry data of each experiment. In the following sections, the results are presented as the logarithms of both ηs
254 and ηr.

3. Results

256 ### *3.1. Liquid viscosities of magmas at Piton de la Fournaise.*

The melt composition studied here is reported in Table 1. It is representative of the
258 parental melt feeding the central activity of Piton de la Fournaise (Di Muro et al., 2016; Di Muro et al., 2014; Famin et al., 2009; Villemant et al., 2009). The viscosity measurements
260 of the crystal free liquid are summarized, together with the VFT model fitted to the low and high temperature viscometry data in Figure 1. For comparison we also report viscosity
262 measurements as well as GRD model estimates (Giordano et al., 2008b) of three other

compositions presented in Villeneuve et al. (2008). These span the compositional variety of the Piton de la Fournaise volcano, where SGBa98 is representative of the more evolved and O77 representative of the more primitive melt compositions erupted at Piton de la Fournaise (Albarède et al., 1997; Boivin and Bachèlery, 2009; Famin et al., 2009; Villemant et al., 2009).

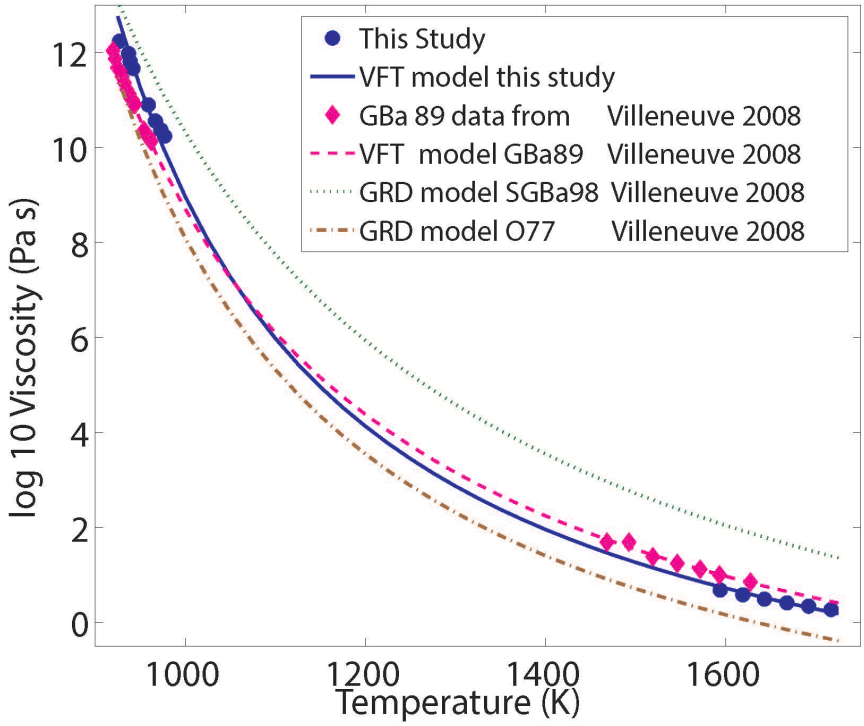

Figure 1: Summary of crystal free liquid viscometry data on Piton lavas. Blue dots represent high temperature CC data and low temperature DSC measurements converted to viscosity, measured for this study. The blue solid line represents the VFT-model fitted to these data. Magenta diamonds and dashed line represent viscometry data from Villeneuve et al. (2008). Green dotted and brown dash-dotted lines represent GRD model curved for compositions SGBa90 and O77 reported in Villeneuve et al. (2008), respectively. Errors are smaller than symbol size.

3.2. Viscosity evolution of the crystallizing suspension

The temperature-dependent viscosity of the Piton de la Fournaise lava, when subjected to varying cooling rates is plotted as absolute and relative viscosity vs. temperature in Figures

2 and 3, respectively; the data are reported as absolute and relative viscosity in Tables 3 and 4, respectively.

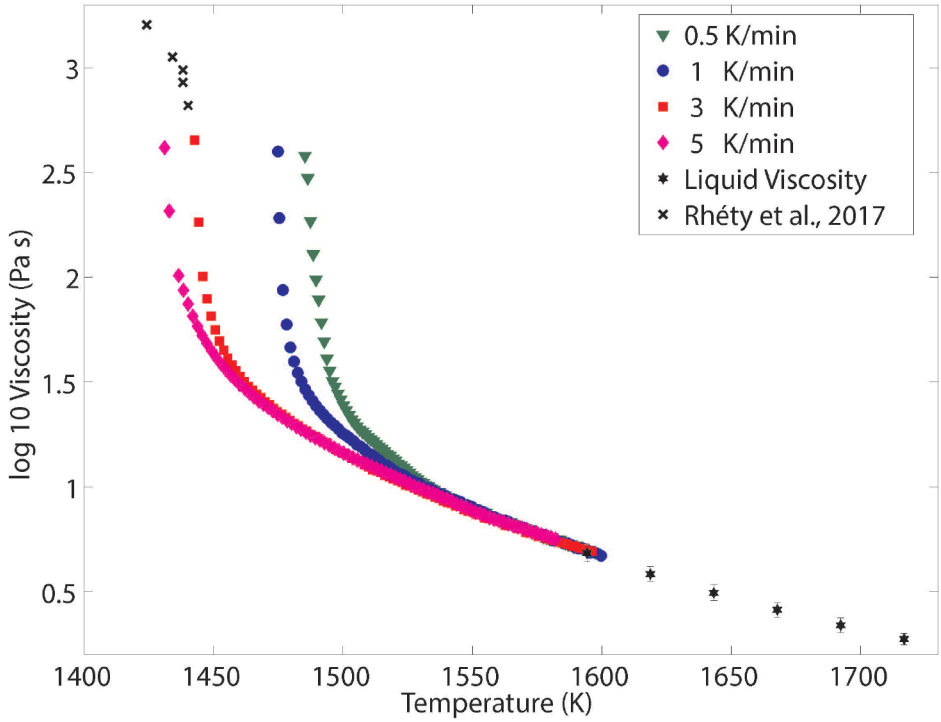

Figure 2: Summary of non-isothermal viscometry data on Piton lavas presented as absolute viscosity. Black stars represent high temperature CC data. Green triangles, blue dots, red squares and magenta diamonds represent constant cooling viscometry data on the evolving suspension at cooling rates of 0.5, 1, 3 and 5 K/min, respectively. Black crosses represent viscosity estimates based on sample textures from (Rhéty et al., 2017). The precision of the viscosity determination is ±3% of the measured value.

The rheological evolution of the lava follows the trend of the pure liquid data (log η_r= 0) up until the point where the influence of crystalline phases (via nucleation and growth of crystals) starts to measurably increase the sample's apparent viscosity. At this deviation, the apparent viscosity of the suspension increases with respect to the theoretical liquid ($\log\eta_r > 0$). This increase in relative viscosity accelerates rapidly as temperature decreases. At higher cooling rates this departure commences at progressively lower temperatures (i.e. higher degrees of undercooling) since crystallisation of the melt is delayed. Further, the nature of this departure is correlated with the imposed cooling rate,

where slower imposed cooling rates result in a steeper rheological departure. This is in agreement with earlier non-isothermal rheological experiments at atmospheric conditions (Giordano et al., 2007; Kolzenburg et al., 2018b; Kolzenburg et al., 2016b).

The crystallization induced rheological departure accelerates continuously until the samples reach the torque limit of the experimental device. This point is close to a specific sub-liquidus temperature, the so-called "rheological cut-off temperature" (T_{cutoff}) at which the sample becomes rheologically immobile and flow ceases. Albeit direct measurements at high viscosities, approaching solidification, are not possible due to mechanical constraints of the experimental setup, the data show that T_{cutoff} shifts systematically to lower temperatures with increasing cooling rate.

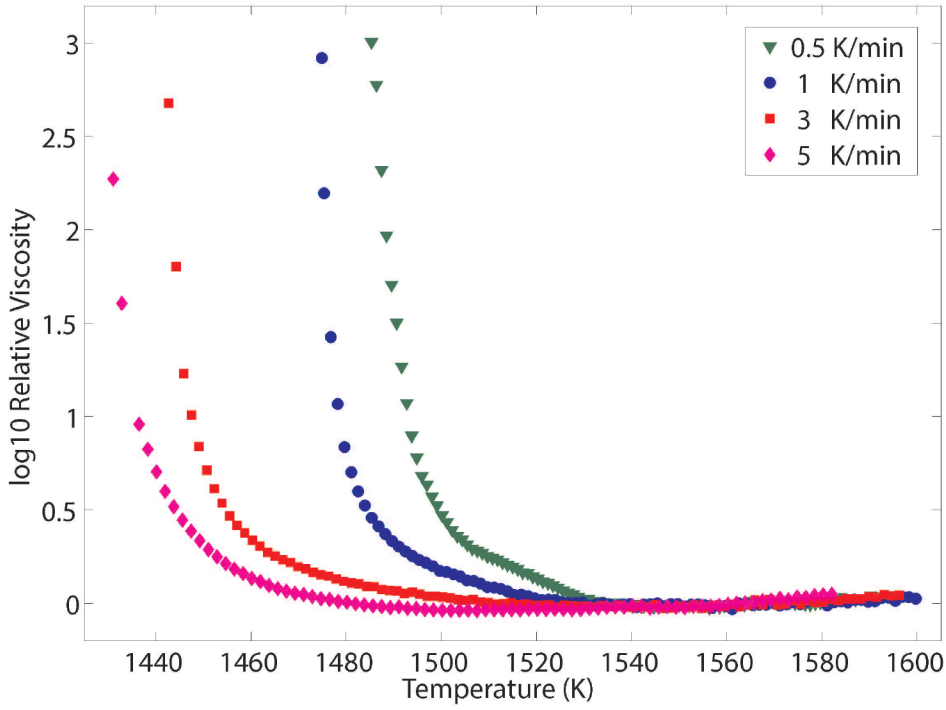

Figure 3: Summary of non-isothermal viscometry data on Piton lavas presented as relative viscosity. Green triangles, blue dots, red squares and magenta diamonds represent constant cooling viscometry data on the evolving suspension at cooling rates of 0.5, 1, 3 and 5 K/min, respectively. The precision of the viscosity determination is ±3% of the measured value.

4. Discussion

4.1. Implications for magma transport and lava emplacement at Piton de la Fournaise

The data reported in Figure 2 show that the viscosity measurements presented here are in good agreement with the down-flow viscosities calculated by Rhéty et al. (2017). The latter study estimated the bulk lava viscosity of the 2007 lava flow using the texture-based approach for multiphase rheology presented in Phan-Thien and Pham (1997) in combination with the temperature-dependent melt viscosity model reported in Villeneuve et al. (2008). Direct comparison with our measurements is consistent with down-flow cooling rates of 3 to 5 K/min. Rhéty et al. (2017), reconstruct initial cooling rates of 7 K/km that increase down-flow to 42 K/km. Accounting for the average flow channel geometries (i.e. widths between 4 and 30 m and heights between 0.8 and 2 m) reported for the flow zones defined in Rhéty et al. (2017) and the average effusion rate of 54 m^3s^{-1} reported in Staudacher et al. (2009), the distance-dependent cooling rates convert to time-dependent cooling rates of 0.1 to 2 K/min and 0.7 to 12 K/min for the reported values of 7 K/km and 42 K/km, respectively.

Lava cooling rates increase sharply during late stages of flow once the lava leaves the well-insulated transport system (Cashman et al., 1999; Harris et al., 2005; Harris and Rowland, 2009), therefore the lower cooling rates reported in the former studies are likely most representative of the dominant flow phase. Values as low as 0.1 K/min, however, are lower than the cooling rate imposed in the experiments (see viscometry data plotted in Figure 1). We attribute this mismatch to the changes in oxygen fugacity between the experiments, carried out in atmospheric conditions, and the natural lava, being erupted in a more reduced state; see Vlastélic et al. (2016), Pichavant et al. (2016) and references

therein. The pre-eruptive fO_2 for PdF magmas is estimated at ~NNO-0.5 and shallow level degassing of SO_2 and H_2O might further decrease the oxygen fugacity; this is suggested by late stabilization of sulphides at shallow level; see (Vlastélic et al., 2016). According to the data presented in Kolzenburg et al. (2018a) such a shift in fO_2 may result in a decrease of the rheologic departure and T_{cutoff} of ~ 40 to 80℃. When accounting for such a ~40-80 K decrease in the rheologic departure due to varying fO_2 conditions, the reconstructed cooling rates of 0.1 to 2 K/min match with the experimental measurements, indicating that the erupted lava did not undergo efficient redox equilibration during subaerial flow.

4.2. Towards forecasting the rheological cut-off temperature (T_{cutoff}).

The decrease in T_{cutoff} with increasing cooling rate is a result of the balance between crystal nucleation and growth rate and the rate of undercooling experienced by the sample (Kolzenburg et al., 2018a; Kolzenburg et al., 2016b). There are two dominant mechanical constraints of the experimental apparatus that do not allow to continue the rheological measurement beyond the maximum viscosity values presented here: 1) the torque limit of the rheometer head and 2) the fact that the crucible containing the experimental sample may start to slip and rotate in its holder at high torque, rendering the measured torque data invalid. Here we present a new, numerical, approach that uses the self-accelerating nature of the rheological departure to forecast the T_{cutoff} value (i.e. the temperature at which the sample becomes rheologically immobile and infinite viscosity is reached) of the lavas under the imposed experimental conditions. This approach follows the failure forecast method (FFM) adopted in volcano seismology and material science to predict failure of a material based on the rate of increase in seismic energy released prior to failure (Voight, 1988; Voight, 1989).

360 It is based on the following equation:

$$\frac{d^2\Omega}{dt^2} = A\left(\frac{d\Omega}{dt}\right)^{\propto} \qquad \text{Equation (1)}$$

362 where $d^2\Omega/dt^2$ and $d\Omega/dt$ are the acceleration and rate of the phenomenon being monitored, and A and α are empirical parameters. For predicting rock failure, this equation 364 is commonly simplified to describe only peaks in signal acceleration rate using a constant α=2, as shown in Kilburn (2003) and Lavallée et al. (2008) resulting in:

366 $$\left(\frac{d\Omega}{dt}\right)^{-1} = \left(\frac{d\Omega}{dt}\right)_0^{-1} - A(t - t_0) \qquad \text{Equation (2)}$$

where t is time, and $(d\Omega/dt)_0$ is the value of $(d\Omega/dt)$ when $t= t_0$. The FFM utilizes 368 the production rate of a precursory phenomena and correlates its acceleration to the point at which the process reaches an uncontrolled (i.e. runaway) state. This state is reached at an 370 infinite $d\Omega/dt$, that implies an uncontrolled rate of change and, thereby, the point at which the monitored process reaches infinite velocity. The forecasting potential of Eq. 1 lies in its 372 potential for describing the rate at which $d\Omega/dt$ approaches uncontrolled conditions. Plotting inverse rate against time returns a negative linear trend, where the time at which 374 the inverse rate equals zero corresponds to the uncontrolled condition when $d\Omega/dt$ tends to infinity (Kilburn, 2003; Lavallée et al., 2008). This point can then be obtained by simple 376 linear extrapolation of the measured trend to the time axis. In volcano seismology or laboratory experimentation on the brittle ductile transition of magma, the precursory signal 378 of the fracturing and failure phenomena are for example, seismicity rate, acoustic emission rate or seismic energy release. The forecasting potential for volcanic eruptions has been 380 demonstrated on seismic data from active volcanoes (Kilburn, 2003; Kilburn and Voight, 1998) as well as for experiments on natural lavas at the brittle ductile transition (Lavallée

et al., 2008). For further details see also (Cornelius and Voight, 1995; De la Cruz-Reyna and Reyes-Dávila, 2001; Tokarev, 1963).

In the case of crystallizing lava that experiences ever increasing undercooling, the precursory signal to T_{cutoff} (i.e. the lava becomes rheologically immobile resulting from an accelerating crystallization rate) is the rate of increase in suspension viscosity. This is measured as a function of temperature instead of time. The formulation for forecasting then reads $d\eta/dT$ (instead of $d\Omega/dt$), where η and T are the effective suspension viscosity and temperature, respectively. The temperature at which the inverse rate reaches zero corresponds to the uncontrolled condition when $d\Omega/dT$ tends to infinity. In Figure 4 we present plots of the inverse rate of viscosity increase against temperature.

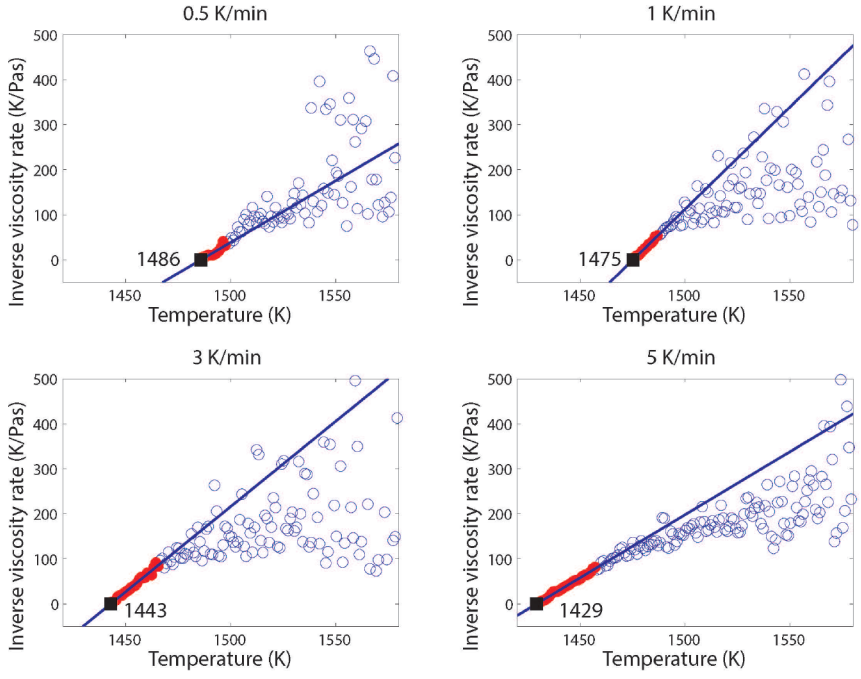

Figure 4: Plot of viscosity acceleration rate vs Temperature. Data for cooling rates of 0.5, 1, 3 and 5 K/min are plotted in subplots a, b, c and d, respectively. Blue open circles represent the experimental data interpolated at 1 degree intervals. Red filled circles represent the linear part of the data used to fit the linear model of viscosity acceleration for extrapolation to T_{cutoff}. Black squares represent the predicted T_{cutoff} (i.e. $d\Omega/dT = \infty$). The precision of the viscosity determination is ±3% of the measured value.

The data plot randomly at high temperatures, where the acceleration is small (i.e. large numbers of inverse acceleration). Once crystallization sets in, the acceleration of the measured suspension viscosity increases, forcing the data to converge on a negative linear trend. Thus, T_{cutoff} can be obtained by simple linear extrapolation of the measured trend to the temperature axis.

Figure 5 reports the values forecasted using this method as a function of cooling rate. We fit a power law model to the predicted T_{cutoff} values that describes the data with an R-squared value of 0.9881.

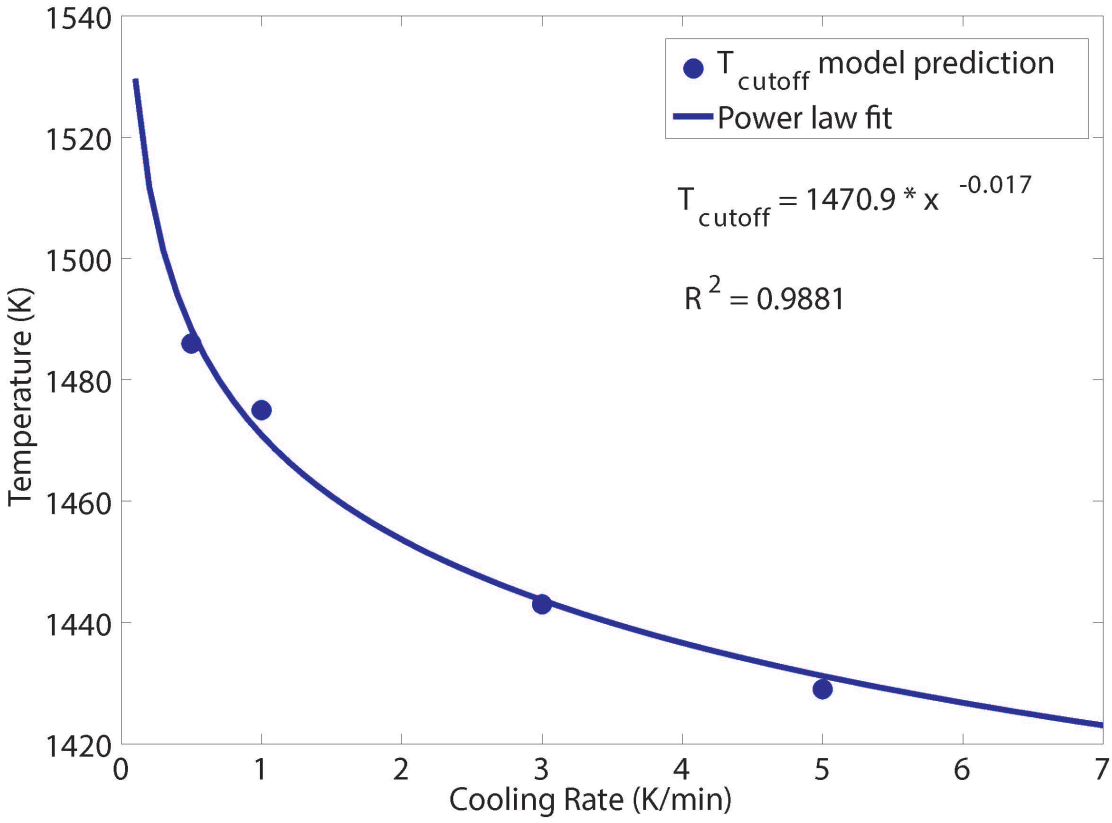

Figure 5: Plot of the predicted T_{cutoff} temperatures as a function of cooling rate. Blue circles represent the forecasted values from the data in figure 4 for cooling rates of 0.5, 1, 3 and 5 K/min. the blue solid line represents a power law model fitted to these data describing the T_{cutoff} lava immobilization threshold as a function of cooling rate. Errors are smaller than symbol size.

Extrapolation of the data using this model suggests that further increasing cooling rate would result in a smaller effect of cooling rate on this rheological threshold, whereas decreasing cooling rates would further increase the temperature at which this threshold is reached. This is due to the longer time spent at higher temperatures, allowing for crystal growth approaching near equilibrium conditions. However, since the model describes a crystallization induced rheological threshold, it is important to note that the model is only valid at sub-liquidus temperatures and non-equilibrium conditions (i.e. at constant cooling rates).

Incorporating T_{cutoff} measurements in lava-flow models will allow for the concept of yield strength to be replaced by a melt specific rheological T_{cutoff} that is dependent on composition, shear- and cooling-rate (Kolzenburg et al., 2018a; Kolzenburg et al., 2018b; Kolzenburg et al., 2016b). The concepts of yield strength or other arbitrary or empirically chosen parameters such as fixed crystal contents, temperature or degrees of undercooling have been introduced in numerical simulations of lava flows (especially in cellular automata type models; e.g. (Miyamoto and Sasaki, 1997)) in order to ascribe a halting criterion to a modelled lava parcel. It has also been introduced as a rheologic criterion in planetary sciences for the derivation of rheological parameters from flow morphology, derived from experiments using analogue materials that possess yield strength e.g. (Fink and Griffiths, 1990; Hulme, 1974). In these analogue experiments these materials were chosen in order to mimic the development of a crust during cooling and they do not to represent actual flow rheology as demonstrated in Kolzenburg et al. (2018c). T_{cutoff} data would therefore represent a more realistic description of the lavas rheological evolution and therewith better ability to forecast their emplacement and flow cessation. The new approach to predict flow cessation may eventually be combined with satellite remote

sensing data of the thermal evolution of lava flows such as presented in Coppola et al. (2013) to provide near real time assessment and forecasting of flow evolution.

5. Conclusions

In conclusion, we find that:

1. Cooling rate exerts a first order control on the sub liquidus rheological evolution of the high Mg Basalt from Piton de la Fournaise through its influence on the melt crystallization-kinetics.
2. The failure forecasting method (FFM) can be adopted to extrapolate disequilibrium viscometry data beyond the mechanical constraints of the experimental apparatus for prediction of the lavas T_{cutoff}.
3. Modelling of magmatic flow behaviour requires melt-composition specific flow- and crystallization-models describing T_{cutoff}.
4. Developing a systematic process understanding of the non-equilibrium rheology of natural silicate melt suspensions requires an expanded database of dynamic measurements such as those presented here.
5. Implementation of data on the dynamic rheological evolution of magma during ascent in dykes and during the emplacement of lavas in computational models would allow to more accurately constrain the results of physical property based magma and lava transport models.

Acknowledgements

We would like to thank Werner Ertel-Ingrisch and Kai-Uwe Hess for support in the Laboratory and interesting discussions during the experimental campaign. Fabio Arzilli and an anonymous reviewer are thanked for constructive comments that helped improve

460 the manuscript. Stephan Kolzenburg and Daniele Giordano acknowledge support from Fondazione CRT, Compagnia San Paolo, an ERASMUS Traineeship and the University of
462 Torino. Stephan Kolzenburg further acknowledges financial support from a H2020 Marie Skłodowska-Curie fellowship DYNAVOLC – No.795044. DBD wishes to acknowledge
464 the support of ERC Advanced Researcher Grant EVOKES – No.247076. ADM was supported by the Agence National de la Recherche through project ANR-LAVA (ANR Program:
466 DS0902 2016; Project: ANR-16 CE39-0009).

9. References

468

Albarède, F. et al., 1997. The geochemical regimes of Piton de la Fournaise volcano
470 (Réunion) during the last 530 000 years. Journal of Petrology, 38(2): 171-201.
Arzilli, F., Carroll, M.R., 2013. Crystallization kinetics of alkali feldspars in cooling and
472 decompression-induced crystallization experiments in trachytic melt. Contributions to Mineralogy and Petrology, 166(4): 1011-1027.
474 Barberi, F., Brondi, F., Carapezza, M.L., Cavarra, L., Murgia, C., 2003. Earthen barriers to control lava flows in the 2001 eruption of Mt. Etna. J. Volcanol. Geotherm. Res.,
476 123(1–2): 231-243.
Belousov, A., Belousova, M., 2018. Dynamics and viscosity of 'a'a and pahoehoe lava
478 flows of the 2012–2013 eruption of Tolbachik volcano, Kamchatka (Russia). Bulletin of Volcanology, 80(1): 6.
480 Boivin, P., Bachèlery, P., 2009. Petrology of 1977 to 1998 eruptions of Piton de la Fournaise, La Réunion Island. Journal of volcanology and geothermal research,
482 184(1): 109-125.
Cashman, K.V. et al., 2013. How lava flows: New insights from applications of lidar
484 technologies to lava flow studies. Geosphere, 9(6): 1664-1680.
Cashman, K.V., Thornber, C., Kauahikaua, J.P., 1999. Cooling and crystallization of lava
486 in open channels, and the transition of Pāhoehoe Lava to 'A'ā. Bulletin of Volcanology, 61(5): 306-323.
488 Chevrel, M.O. et al., 2015. Viscosity measurements of crystallizing andesite from Tungurahua volcano (Ecuador). Geochemistry, Geophysics, Geosystems.
490 Chevrel, M.O. et al., 2018. The viscosity of pāhoehoe lava: in situ syn-eruptive measurements from Kilauea, Hawaii 2. Earth and Planetary Science Letters.
492 Coish, R., Taylor, L.A., 1979. The effects of cooling rate on texture and pyroxene chemistry in DSDP Leg 34 basalt: a microprobe study. Earth and planetary science
494 letters, 42(3): 389-398.
Coppola, D., Laiolo, M., Piscopo, D., Cigolini, C., 2013. Rheological control on the radiant
496 density of active lava flows and domes.
Cornelius, R.R., Voight, B., 1995. Graphical and PC-software analysis of volcano eruption
498 precursors according to the Materials Failure Forecast Method (FFM). Journal of Volcanology and Geothermal Research, 64(3-4): 295-320.

500 De la Cruz-Reyna, S., Reyes-Dávila, G.A., 2001. A model to describe precursory material-failure phenomena: applications to short-term forecasting at Colima volcano,
502 Mexico. Bulletin of Volcanology, 63(5): 297-308.
Di Genova, D., Caracciolo, A., Kolzenburg, S., 2018. Measuring the degree of
504 "nanotilization" of volcanic glasses: Understanding syn-eruptive processes recorded in melt inclusions. Lithos, 318-319: 209-218.
506 Di Muro, A. et al., 2016. Magma degassing at Piton de la Fournaise volcano, Active Volcanoes of the Southwest Indian Ocean. Springer, pp. 203-222.
508 Di Muro, A. et al., 2014. The shallow plumbing system of Piton de la Fournaise Volcano (La Reunion Island, Indian Ocean) revealed by the major 2007 caldera-forming
510 eruption. Journal of Petrology, 55(7): 1287-1315.
Dingwell, D., 1991. Redox viscometry of some Fe-bearing silicate melts. American
512 Mineralogist, 76(9-10): 1560-1562.
Dingwell, D.B., 1986. Viscosity-temperature relationships in the system Na2Si2O5-
514 Na4Al2O5. Geochimica et Cosmochimica Acta, 50(6): 1261-1265.
Dingwell, D.B., 1990. Shear viscosities of galliosilicate liquids. American
516 Mineralogist(11-12): 1231-1237.
Dingwell, D.B., 1992. Shear viscosity of alkali and alkaline earth titanium silicate liquids.
518 American Mineralogist(3-4): 270-274.
Dingwell, D.B., Virgo, D., 1987. The effect of oxidation state on the viscosity of melts in
520 the system Na_2O-FeO-Fe_2O_3-SiO_2. Geochimica et Cosmochimica Acta, 51(2): 195-205.
522 Dingwell, D.B., Virgo, D., 1988. Viscosities of melts in the Na_2O-FeO-Fe_2O_3-SiO_2 system and factors controlling relative viscosities of fully polymerized silicate melts.
524 Geochimica et Cosmochimica Acta(2): 395-403.
Dragoni, M., Bonafede, M., Boschi, E., 1986. Downslope flow models of a Bingham
526 liquid: implications for lava flows. Journal of Volcanology and Geothermal Research, 30(3-4): 305-325.
528 Einarsson, T., 1949. Studies of the Pleistocene in Eyjafjörður, Middle Northern Iceland. Prentsmiðjan Leiftur.
530 Famin, V., Welsch, B., Okumura, S., Bachèlery, P., Nakashima, S., 2009. Three differentiation stages of a single magma at Piton de la Fournaise volcano (Reunion
532 hot spot). Geochemistry, Geophysics, Geosystems, 10(1).
Farquharson, J., James, M., Tuffen, H., 2015. Examining rhyolite lava flow dynamics
534 through photo-based 3D reconstructions of the 2011–2012 lava flowfield at Cordón-Caulle, Chile. Journal of Volcanology and Geothermal Research, 304: 336-
536 348.
Favalli, M. et al., 2010. Evolution of an active lava flow field using a multitemporal
538 LIDAR acquisition. Journal of Geophysical Research: Solid Earth (1978–2012), 115(B11).
540 Fink, J.H., Griffiths, R.W., 1990. Radial spreading of viscous-gravity currents with solidifying crust. Journal of Fluid Mechanics, 221: 485-509.
542 Fretzdorff, S., Haase, K., 2002. Geochemistry and petrology of lavas from the submarine flanks of Réunion Island (western Indian Ocean): implications for magma genesis
544 and the mantle source. Mineralogy and Petrology, 75(3-4): 153-184.
Gamble, R.P., Taylor, L.A., 1980. Crystal/liquid partitioning in augite: effects of cooling
546 rate. Earth and planetary science letters, 47(1): 21-33.

Gauthier, F., 1973. Mount Etna and the 1971 eruption-Field and laboratory studies of the rheology of Mount Etna lava. Phil. Trans. R. Soc. Lond. A, 274(1238): 83-98.

Giordano et al., 2015. Heat capacity of hydrous trachybasalt from Mt Etna: comparison with $CaAl_2Si_2O_8$ (An)–$CaMgSi_2O_6$ (Di) as basaltic proxy compositions. Contributions to Mineralogy and Petrology, 170(5-6): 1-23.

Giordano, Potuzak, M., Romano, C., Dingwell, D.B., Nowak, M., 2008a. Viscosity and glass transition temperature of hydrous melts in the system $CaAl_2Si_2O_8$–$CaMgSi_2O_6$. Chemical Geology, 256(3–4): 203-215.

Giordano, Russell, J.K., Dingwell, D.B., 2008b. Viscosity of magmatic liquids: A model. Earth Planet. Sci. Lett., 271(1–4): 123-134.

Giordano, D. et al., 2007. Thermo-rheological magma control on the impact of highly fluid lava flows at Mt. Nyiragongo. Geophys. Res. Lett., 34(6).

Giordano, D., Russell, J., 2017. The heat capacity of hydrous multicomponent natural melts and glasses. Chemical Geology, 461: 96-103.

Gottsmann, J., Giordano, D., Dingwell, D.B., 2002. Predicting shear viscosity during volcanic processes at the glass transition: a calorimetric calibration. Earth and Planetary Science Letters, 198(3): 417-427.

Hallworth, M., Huppert, H., Sparks, R., 1987. A laboratory simulation of basaltic lava flows. Mod. Geol, 11: 93-107.

Hammer, J.E., 2006. Influence of fO 2 and cooling rate on the kinetics and energetics of Fe-rich basalt crystallization. Earth and Planetary Science Letters, 248(3): 618-637.

Harris, A., Bailey, J., Calvari, S., Dehn, J., 2005. Heat loss measured at a lava channel and its implications for down-channel cooling and rheology. SPECIAL PAPERS-GEOLOGICAL SOCIETY OF AMERICA, 396: 125.

Harris, A., Rowland, S., 2009. Effusion rate controls on lava flow length and the role of heat loss: a review. Studies in volcanology: the legacy of George Walker. Special Publications of IAVCEI, 2: 33-51.

Harris, A.J., Rowland, S., 2001. FLOWGO: a kinematic thermo-rheological model for lava flowing in a channel. Bulletin of Volcanology, 63(1): 20-44.

Hess, K.-U., Dingwell, D.B., 1996. Viscosities of hydrous leucogranitic melts: A non-Arrhenian model. American Mineralogist, 81: 1297-1300.

Hess, K., Dingwell, D., Webb, S., 1995. The influence of excess alkalis on the viscosity of a haplogranitic melt. American Mineralogist, 80(3): 297-304.

Hulme, G., 1974. The Interpretation of Lava Flow Morphology. Geophysical Journal International, 39(2): 361-383.

Ishibashi, H., Sato, H., 2007. Viscosity measurements of subliquidus magmas: Alkali olivine basalt from the Higashi-Matsuura district, Southwest Japan. Journal of Volcanology and Geothermal Research, 160(3–4): 223-238.

James, M., Robson, S., 2014. Sequential digital elevation models of active lava flows from ground-based stereo time-lapse imagery. ISPRS Journal of Photogrammetry and Remote Sensing, 97: 160-170.

Kilburn, C.R., 2003. Multiscale fracturing as a key to forecasting volcanic eruptions. Journal of Volcanology and Geothermal Research, 125(3-4): 271-289.

Kilburn, C.R., Voight, B., 1998. Slow rock fracture as eruption precursor at Soufriere Hills volcano, Montserrat. Geophysical Research Letters, 25(19): 3665-3668.

592 Kolzenburg, S., Di Genova, D., Giordano, D., Hess, K.U., Dingwell, D.B., 2018a. The effect of oxygen fugacity on the rheological evolution of crystallizing basaltic
594 melts. Earth and Planetary Science Letters, 487: 21-32.
Kolzenburg, S. et al., 2016a. Rapid Updating and Improvement of Airborne LIDAR DEMs
596 Through Ground-Based SfM 3-D Modeling of Volcanic Features. IEEE Transactions on Geoscience and Remote Sensing, PP(99): 1-13.
598 Kolzenburg, S., Giodano, D., Hess, K.U., Dingwell, D.B., 2018b. Shear Rate-Dependent Disequilibrium Rheology and Dynamics of Basalt Solidification. Geophysical
600 Research Letters, 45(13): 6466-6475.
Kolzenburg, S., Giordano, D., Cimarelli, C., Dingwell, D.B., 2016b. In Situ thermal
602 characterization of cooling/crystallizing lavas during rheology measurements and implications for lava flow emplacement. Geochimica et Cosmochimica Acta(195):
604 244-258.
Kolzenburg, S., Giordano, D., Thordarson, T., Höskuldsson, A., Dingwell, D.B., 2017. The
606 rheological evolution of the 2014/2015 eruption at Holuhraun, central Iceland. Bulletin of Volcanology, 79(6): 45.
608 Kolzenburg, S., Jaenicke, J., Münzer, U., Dingwell, D.B., 2018c. The effect of inflation on the morphology-derived rheological parameters of lava flows and its implications
610 for interpreting remote sensing data - A case study on the 2014/2015 eruption at Holuhraun, Iceland. Journal of Volcanology and Geothermal Research, 357: 200-
612 212.
Kouchi, A., Tsuchiyama, A., Sunagawa, I., 1986. Effect of stirring on crystallization
614 kinetics of basalt: texture and element partitioning. Contributions to Mineralogy and Petrology, 93(4): 429-438.
616 Lavallée, Y. et al., 2008. Seismogenic lavas and explosive eruption forecasting. Nature, 453(7194): 507-510.
618 Lofgren, G., 1980. Experimental studies on the dynamic crystallization of silicate melts. Physics of magmatic processes, 487.
620 Long, P.E., Wood, B.J., 1986. Structures, textures, and cooling histories of Columbia River basalt flows. Geological Society of America Bulletin, 97(9): 1144-1155.
622 Meerlender, G., 1975. Erstes Standardglas der Deutschen Glastechnischen Gesellschaft und Realisierung der Viskositätsskala bei hohen Temperaturen. Rheologica Acta,
624 14(3): 279-290.
Miyamoto, H., Sasaki, S., 1997. Simulating lava flows by an improved cellular automata
626 method. Comput. Geosci., 23(3): 283-292.
Mysen, B.R.O., Virgo, D., 1978. Influence of pressure, temperature, and bulk composition
628 on melt structures in the system NaAlSi< 2) O< 6)-NaFe> 3+) Si< 2) O< 6). American Journal of Science, 278(9): 1307-1322.
630 Panov, V.K., Slezin, Y.B., Storcheus, A.V., 1988. Mechanical properties of lava extruded in the 1983 Predskazanny eruption (Klyuchevskoi volcano). J Volcanol Seismol, 7:
632 25-37.
Phan-Thien, N., Pham, D., 1997. Differential multiphase models for polydispersed
634 suspensions and particulate solids. Journal of Non-Newtonian Fluid Mechanics, 72(2-3): 305-318.
636 Pichavant, M., Brugier, Y., Di Muro, A., 2016. Petrological and experimental constraints on the evolution of Piton de la Fournaise magmas, Active Volcanoes of the
638 Southwest Indian Ocean. Springer, pp. 171-184.

Pinkerton, H., 1987. Factors affecting the morphology of lava flows. Endeavour, 11(2): 73-79.

Pinkerton, H., 1994. Rheological and related properties of lavas. Etna: Magma and Lava Flow Modeling and Volcanic System Definition Aimed at Hazard Assessment: 76-89.

Pinkerton, H., Norton, G., 1995. Rheological properties of basaltic lavas at sub-liquidus temperatures: laboratory and field measurements on lavas from Mount Etna. Journal of Volcanology and Geothermal Research, 68(4): 307-323.

Pinkerton, H., Sparks, R.S.J., 1978. Field measurements of the rheology of lava. Nature, 276(5686): 383-385.

Pouchou, J.-L., Pichoir, F., 1991. Quantitative analysis of homogeneous or stratified microvolumes applying the model "PAP", Electron probe quantitation. Springer, pp. 31-75.

Rhéty, M. et al., 2017. A comparison of cooling-and volume-limited flow systems: Examples from channels in the Piton de la Fournaise April 2007 lava flow field. Geochemistry, Geophysics, Geosystems.

Robert, B. et al., 2014. Textural and rheological evolution of basalt flowing down a lava channel. Bulletin of Volcanology, 76(6): 1-21.

Sato, H., 2005. Viscosity measurement of subliquidus magmas:1707 basalt of Fuji volcano. Journal of Mineralogical and Petrological Sciences, 100(4): 133-142.

Sehlke, A. et al., 2014. Pahoehoe to `a`a transition of Hawaiian lavas: an experimental study. Bulletin of Volcanology, 76(11): 1-20.

Shaw, H., Wright, T., Peck, D., Okamura, R., 1968. The viscosity of basaltic magma; an analysis of field measurements in Makaopuhi lava lake, Hawaii. American Journal of Science, 266(4): 225-264.

Soldati, A., Sehlke, A., Chigna, G., Whittington, A., 2016. Field and experimental constraints on the rheology of arc basaltic lavas: the January 2014 Eruption of Pacaya (Guatemala). Bulletin of Volcanology, 78(6): 1-19.

Staudacher, T. et al., 2009. The April 2007 eruption and the Dolomieu crater collapse, two major events at Piton de la Fournaise (La Réunion Island, Indian Ocean). Journal of Volcanology and Geothermal Research, 184(1): 126-137.

Tammann, G., Hesse, W., 1926. Die Abhängigkeit der Viscosität von der Temperatur bie unterkühlten Flüssigkeiten. Zeitschrift für anorganische und allgemeine Chemie, 156(1): 245-257.

Tokarev, P., 1963. On a possibility of forecasting of Bezymianny volcano eruptions according to seismic data. Bulletin Volcanologique, 26(1): 379-386.

Vetere, F. et al., 2013. Intrinsic solidification behaviour of basaltic to rhyolitic melts: a cooling rate experimental study. Chemical Geology, 354: 233-242.

Villemant, B., Salaün, A., Staudacher, T., 2009. Evidence for a homogeneous primary magma at Piton de la Fournaise (La Réunion): A geochemical study of matrix glass, melt inclusions and Pélé's hairs of the 1998–2008 eruptive activity. Journal of Volcanology and Geothermal Research, 184(1): 79-92.

Villeneuve, N., Neuville, D.R., Boivin, P., Bachèlery, P., Richet, P., 2008. Magma crystallization and viscosity: a study of molten basalts from the Piton de la Fournaise volcano (La Réunion island). Chemical Geology, 256(3): 242-251.

684 Vlastélic, I. et al., 2016. Origin and fate of sulfide liquids in hotspot volcanism (La Réunion): Pb isotope constraints from residual Fe–Cu oxides. Geochimica et
686 Cosmochimica Acta, 194: 179-192.
Voight, B., 1988. A method for prediction of volcanic eruptions. Nature, 332(6160): 125.
688 Voight, B., 1989. A relation to describe rate-dependent material failure. Science, 243(4888): 200-203.
690 Vona, A., Romano, C., Dingwell, D.B., Giordano, D., 2011. The rheology of crystal-bearing basaltic magmas from Stromboli and Etna. Geochimica et Cosmochimica
692 Acta, 75(11): 3214-3236.
Vona, A., Romano, C., Giordano, D., Russell, J.K., 2013. The multiphase rheology of
694 magmas from Monte Nuovo (Campi Flegrei, Italy). Chemical Geology, 346(0): 213-227.
696 Walker, D., Kirkpatrick, R., Longhi, J., Hays, J., 1976. Crystallization history of lunar picritic basalt sample 12002: phase-equilibria and cooling-rate studies. Geological
698 Society of America Bulletin, 87(5): 646-656.

700

Tables

702

Table 1:

Oxide	*Wt % Oxide*
SiO_2	48.56
TiO_2	2.40
Al_2O_3	12.15
FeO	12.19
MnO	0.20
MgO	11.61
CaO	9.76
Na_2O	2.33
K_2O	0.56
P_2O_5	0.25
analytical total	99.76

EPMA analysis of major element components as oxides; Data is normalized to 100 wt%

Table 2

Temperature (K)	Temperature (C)	log η (Pa s)	Standard deviation
1717	1444	0.27	0.03
1692	1419	0.34	0.03
1668	1395	0.41	0.04
1643	1370	0.49	0.04
1619	1346	0.58	0.04
1594	1321	0.68	0.04
977	704	10.24	0.17
973	700	10.37	0.17
967	694	10.56	0.15
959	686	10.90	0.14
942	669	11.67	0.26
939	666	11.81	0.25
937	664	11.98	0.24
927	654	12.24	0.24
	A	-3.77	
	B	4163.79	
	C	673.18	

704

Table 3: Summary of absolute viscosity measurements for all experiments. For simplicity we report interpolated values of the experimental data at equal temperature steps with exception of the final datapoint for some experiments; highlighted in grey. Temperatures related to those points are reported in the last two rows in Kelvin and Celsius, respectively.

Cooling Rate (K/min)		**0.5**	**1**	**3**	**5**
Shear Rate (sec^{-1})		**0.77**	**0.77**	**0.77**	**0.77**
T (K)	T (C)	log η (Pa s)			
1573	1300	0.79	0.79	0.78	0.78
1568	1295	0.81	0.81	0.80	0.81
1563	1290	0.83	0.84	0.81	0.83
1558	1285	0.85	0.86	0.84	0.85
1553	1280	0.89	0.89	0.87	0.87
1548	1275	0.91	0.91	0.89	0.90
1543	1270	0.94	0.94	0.91	0.92
1538	1265	0.96	0.96	0.94	0.95
1533	1260	1.00	0.99	0.97	0.98
1528	1255	1.04	1.02	0.99	1.00
1523	1250	1.10	1.06	1.02	1.03
1518	1245	1.15	1.09	1.05	1.06
1513	1240	1.20	1.14	1.08	1.09
1508	1235	1.26	1.18	1.11	1.11
1503	1230	1.32	1.23	1.14	1.14
1498	1225	1.44	1.28	1.17	1.17
1493	1220	1.66	1.34	1.21	1.21
1488	1215	2.16	1.41	1.25	1.24
1483	1210	2.58	1.53	1.29	1.28
1478	1205		1.78	1.33	1.32
1473	1200		2.60	1.37	1.36
1468	1195			1.43	1.40
1463	1190			1.48	1.46
1458	1185			1.56	1.51
1453	1180			1.67	1.58
1448	1175			1.86	1.67
1443	1170			2.54	1.78
1438	1165			2.65	1.94
1433	1160				2.28
1428	1155				2.62
T Final	K	1485	1475	1443	1431
Datapoint	C	1212	1202	1170	1158

706

Table 4: Summary of the calculated relative viscosity for all experiments. For simplicity we report interpolated values of the experimental data at equal temperature steps with exception of the final datapoint for some experiments; highlighted in grey. Temperatures related to those points are reported in the last two rows in Kelvin and Celsius, respectively.

Cooling Rate (K/min)		**0.5**	**1**	**3**	**5**
Shear Rate (sec^{-1})		**0.77**	**0.77**	**0.77**	**0.77**
T (K)	T (C)	log η (Pa s)			
1573	1300	0.01	0.00	0.01	0.02
1568	1295	0.00	-0.01	0.00	0.01
1563	1290	-0.01	0.00	-0.02	0.00
1558	1285	-0.02	-0.01	-0.01	-0.01
1553	1280	-0.01	-0.01	-0.01	-0.02
1548	1275	-0.01	-0.01	-0.03	-0.02
1543	1270	-0.01	-0.01	-0.02	-0.02
1538	1265	-0.01	-0.01	-0.02	-0.02
1533	1260	0.01	0.00	-0.02	-0.03
1528	1255	0.04	0.00	-0.02	-0.04
1523	1250	0.10	0.02	-0.01	-0.03
1518	1245	0.16	0.04	-0.01	-0.03
1513	1240	0.22	0.07	0.00	-0.04
1508	1235	0.28	0.11	0.01	-0.04
1503	1230	0.36	0.15	0.02	-0.04
1498	1225	0.57	0.20	0.04	-0.04
1493	1220	1.00	0.27	0.06	-0.03
1488	1215	2.07	0.37	0.07	-0.02
1483	1210	3.01	0.56	0.10	-0.01
1478	1205		1.09	0.13	0.01
1473	1200		2.92	0.16	0.03
1468	1195			0.22	0.06
1463	1190			0.28	0.10
1458	1185			0.39	0.16
1453	1180			0.57	0.24
1448	1175			0.94	0.37
1443	1170			2.41	0.54
1438	1165			2.68	0.84
1433	1160				1.53
1428	1155				2.27
T Final	K	1485	1475	1443	1431
Datapoint	C	1212	1202	1170	1158